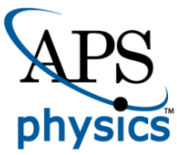



# Local twin domains and tip-voltage-induced domain switching of monoclinic M_{C} phase in Pb(Mg_{1/3}Nb_{2/3})O_{3}-0.34PbTiO_{3} single crystal revealed by piezoresponse force microscopy

Ruixue Wang, Bin Yang, Zhenlin Luo, Enwei Sun, Yuan Sun, Han Xu, Jiangtao Zhao, Limei Zheng, Hua Zhou, Chen Gao, and Wenwu Cao

Phys. Rev. B **94**, 054115 — Published 29 August 2016

DOI: 10.1103/PhysRevB.94.054115

# Local twin domains and tip-voltage-induced domain switching of monoclinic $M_C$ phase in $Pb(Mg_{1/3}Nb_{2/3})O_3$-0.34$PbTiO_3$ single crystal revealed by piezoresponse force microscopy

Ruixue Wang,[1] Bin Yang,[1,*] Zhenlin Luo,[2,*] Enwei Sun,[1] Yuan Sun,[1] Han Xu,[2] Jiangtao Zhao,[2] Limei Zheng,[1] Hua Zhou,[3] Chen Gao,[2] and Wenwu Cao[1,4]

[1]*Condensed Matter Science and Technology Institute, Harbin Institute of Technology, Harbin 150080, China*

[2]*National Synchrotron Radiation Laboratory and CAS Key Laboratory of Materials for Energy Conversion, University of Science and Technology of China, Hefei, Anhui, 230026, China*

[3]*Advanced Photon Source, Argonne National Laboratory, Argonne, Illinois 60439, USA*

[4]*Department of Mathematics and Materials Research Institute, The Pennsylvania State University, University Park, Pennsylvania 16802, USA*

The monoclinic (M) phases in high-performance relaxor-based ferroelectric single crystals have been recognized to be a vital structural factor for the outstanding piezoelectric property. However, due to the complexity of the structure in M phases, the understanding about it is still limited. In this work, the local twin domains and tip-voltage-induced domain switching of monoclinic $M_C$ phase in $Pb(Mg_{1/3}Nb_{2/3})O_3$-0.34$PbTiO_3$ (PMN-0.34PT) single crystal have been intensively investigated by Piezoresponse Force Microscopy (PFM). By theoretically analyzing the experimental patterns of domain walls on $(001)_C$ face, the specific $M_C$ twin domains in the initial annealed state of a selected area have been clarified, and the polarization orientation of the $M_C$ phase in this sample is determined to be at an angle of 29° to the $<001>_C$ directions. In addition, based on the evolution of domains and the motion of domain walls under the step-increased PFM tip DC voltage ($V_{dc}$), the switching process and features of different types of $M_C$ domain variants are visually revealed.

PACS numbers: 77.80.Jk, 77.80.Dj, 77.80.Fm, 61.50.-f

*Corresponding authors:

Bin Yang: binyang@hit.edu.cn, Tel. and Fax Number: 011-86-0451-86402771;

Zhenlin Luo: zlluo@ustc.edu.cn, Tel: +86-13855166031, Fax: +86(6551)514-1078.

## I. INTRODUCTION

Relaxor-based ferroelectric single crystals, such as $Pb(Zn_{1/3}Nb_{2/3})O_3$-$x$$PbTiO_3$ (PZN-$x$PT), $Pb(Mg_{1/3}Nb_{2/3})O_3$- $x$$PbTiO_3$ (PMN-$x$PT) have attracted increasing interest in the past two decades for their excellent ferroelectric and piezoelectric properties [1,2]. In the system of PMN-$x$PT single crystals, the best functional properties appear in the morphotropic phase boundary (MPB) composition [3]. Although the underlying origin of such outstanding properties is still not fully understood, the structure contribution is recognized to be a critical factor [4-8].

During the structural investigation for $ABO_3$ perovskite ferroelectrics, the discovery of a low symmetry Monoclinic (M) phase in $Pb(Zr_{1-x}Ti_x)O_3$ (PZT) had been a significant breakthrough [9]. Rather than a single direction as in rhombohedral (R) and tetragonal (T) phases, the polarization orientation of M phase is confined in a mirror plane. According to the polarization orientation, the M phase was classified into three types: $M_A$, $M_B$ and $M_C$ [10]. For PMN-$x$PT single crystals, the existence of $M_A$, $M_B$ and $M_C$ phases have been confirmed [11-14], and the phase diagram near the MPB was proposed with defined composition range of the M phase [15,16]. The M phase is believed to be closely linked with the enhanced electromechanical performance [17-20]. In addition to the crystal structure, the domain structure also contributes a lot to the unique electromechanical properties for ferroelectrics with the MPB composition [8,21-23]. For ferroelectric single crystals, there were 24 energy equivalent polarization orientations in each kind of M phase, which was far more than that of R and T phases [11]. Therefore, when the compositions approach the MPB, the domain configuration became more complex, and the domain size was miniaturized to nanometer scales [24,25]. The attractive piezoelectric property in the MPB composition sample may

have benefited from the small domain size and the complex multi-domain structure [23,26]. The rotation ability and switching path of the polarization under an electric field may be significant factors for the outstanding piezoelectric property of relaxor-based ferroelectrics single crystals [4,27-29]. What's more, because of the ferroelastic property, the non-180º switching of ferroelectric domains will be accompanied with strain variation. The domain switching paths under electric-field in the single crystal with M phase will be more diversified due to the complexity of domain structure, which makes it attractive to the application in the strain-transfer-based multiferroic heterostructure and the related devices [30-34]. Therefore, in order to understand the domain contribution and to use it better, the switching process of the domains of the M phase should be investigated [35-38].

In recent years, some experimental and theoretical investigations about the crystal and domain structure of M phases were reported [26, 39-44], which gave us more insight into the M phases. However, up to date, there is still significant debate about the structure of the M phase. Although the existence of the M phase was widely accepted, some researchers argue that the M phase domain was actually the adaptive structure of R or T phase nanodomains [45-47], such debate indicates that the understanding of the M phase is still insufficient, and a more visualized and intensive investigation of the structures of the M phase is needed. In our previous work, the coexistence of Mc and T phases and the averaged twinning manner of domains in PMN-0.34PT single crystal have been visually revealed using synchrotron-radiation XRD measurements [48]. But, the local twin domain structures and the polarization orientation of such M phases have not been clarified, and yet the understanding on the domain switching is still limited.

One of the most common methods for the study of domain structure in ferroelectrics is the polarization light microscopy (PLM), but the spatial resolution of PLM is insufficient when exploring small scale features. In the past few years, the optical second harmonic generation (SHG) has been well established as an efficient tool to study the symmetry of the ferroelectrics, and has led to valuable insights on the monoclinic complex domain states [26,49,50]. Transmission electron microscopy (TEM) can achieve even higher resolution, but *in situ* electrical biasing TEM is difficult to perform and the stress state of the specimen may be changed during sample thinning process for TEM. In comparison to PLM, SHG imaging

and TEM, piezoelectric force microscopy (PFM) measurement is able to achieve relatively high spatial resolution in a nondestructive way [51].

Here, in order to gain more insight, the domain pattern and its switching process in a typical relaxor-based ferroelectric single crystal PMN-0.34PT was intensively investigated by vertical PFM (VPFM). Based on the formation rules of domain walls and the scanned VPFM results, the specific twin domains in the initially annealed state of the selected area, and the polarization orientation of the $M_C$ phase in this sample were clarified. Then, according to the evolution of domains and the motion of domain walls under the tip voltage, the switching process and feature of different types of $M_C$ domains were revealed.

## II. EXPERIMENTAL DETAILS

The PMN-0.34PT single crystal used in this research was grown by the modified Bridgman technique [52]. The sample was cut into slice with dimensions of 5 mm//$[100]_C$ × 5 mm//$[010]_C$ × 0.4 mm//$[001]_C$. The $(001)_C$ face of the sample was polished to optical standard for PFM measurement. Because the domain structure is sensitive to stresses, the sample was first annealed without external electric field at 350 °C for 1 h to release the surface stresses involved in the cutting and polish processes. The domain structure was studied via x-ray diffractive 2D/3D reciprocal space mapping (RSM) technique [53, 54]. The 2D-RSM was performed on a Smart lab diffractometer, while the synchrotron x-ray 3D-RSM was conducted at Advanced Photon Source [48]. The ferroelectric domain patterns and switching process were revealed by PFM (Asylum Research, Cypher ES) with conductive probes (Nanoworld, EFM). All of the VPFM scannings in this paper were performed by starting from the lower-left corner and ending at the upper-right corner of each poling area. And the discussions are all based on the results from this poling procedure. Both the x-ray diffractive RSM and VPFM measurements were performed at room temperature.

## III. RESULTS AND DISCUSSION

### 1. Fundamental knowledge and an overview of the experimental results

Figure 1 illustrates the basic knowledge about this sample, and presents an overview of the experimental results. The PMN-0.34PT single crystal is located at the boundary between $M_C$

and T phase in the MPB composition [16]. Fig. 1(a) schematically presents the polarization orientations of the $M_C$ phase, the domains of the $M_C$ phase are classified as $M_C$-a, $M_C$-b and $M_C$-c with the c axis oriented along $[100]_C$, $[010]_C$ and $[001]_C$ directions, respectively. Due to the distortion of crystal lattice, there are four sub-variants for each kind of $M_C$ domain, which are numbered as 1-4 (for example, $M_C$-a1). There are another twelve $M_C$ domain variants with opposite orientations which are not shown in this figure (for example, $M_C$-a$\bar{1}$). Based on the relationship between reciprocal lattice and real-space crystal plane, for the situation when the $M_C$ and T phases are coexist, the (00L) diffraction pattern on H0L reciprocal plane was simulated and presented in Fig. 1(b). On the other hand, the experimental 2D-RSM pattern around (004) Bragg point on H0L reciprocal plane was presented in Fig. 1(c). By the comparison between the experimental and simulation results, the sample was confirmed to be coexistence of $M_C$ and T phase. However, single 2D-RSM pattern is insufficient to reflect the whole characters of the (00L) diffraction spot. Therefore, the synchrotron x-ray diffractive 3D-RSM measurement was performed around (006) Bragg spot, which was discussed in detail previously elsewhere [48]. For the convenience of building a global and basic understanding on the structure of this sample, the relevant results of x-ray diffractive 3D-RSM have been summarized and presented in Fig. 1(d). In this 3D-RSM, the affiliation of each diffraction spot was identified, and based on the tails between different diffraction spots which were marked with violet double-arrows, the $M_C$ twin domains in the sample was roughly determined to be dominated by $M_C$-a/$M_C$-b and $M_C$-c/$M_C$-a1/3 types with a small volume fraction of $M_C$-c/$M_C$-b1/3 type.

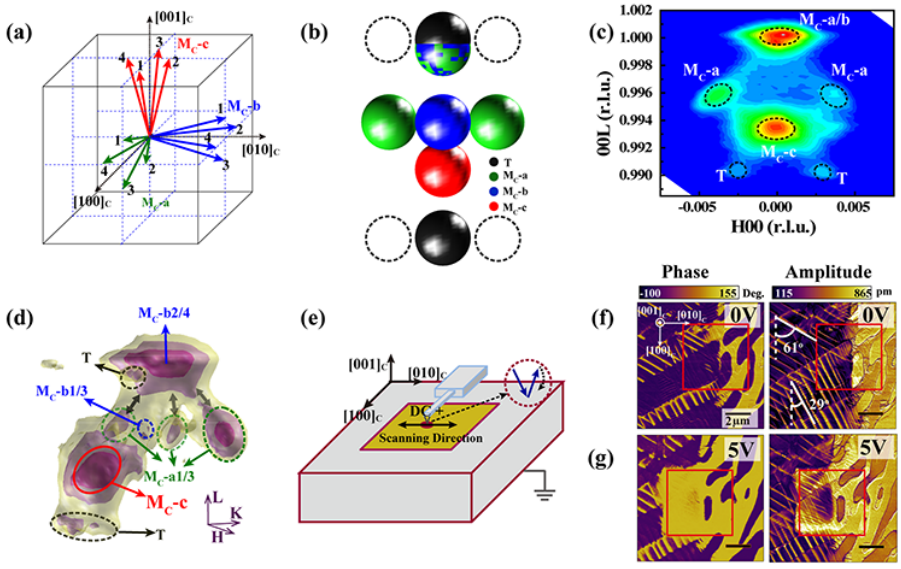


FIG. 1. (Color online) (a) Spontaneous polarization orientations of $M_C$ phase, (b) simulation result of (00L) diffraction pattern on H0L plane, (c) X-ray diffractive 2D-RSM around (004) Bragg spot on H0L reciprocal plane, the diffraction intensity was indicated by different color (low to high: blue, green, yellow, red), (d) synchrotron X-ray diffractive 3D-RSM around (006) diffraction spot (Reuse of [Applied Physics Letters 108, 152905 (2016), Fig. 2f], with the permission of AIP Publishing), the diffraction intensity was indicated by different color (low to high: yellow, pink, purple). (e) Schematic diagram of PFM setup, VPFM phase and amplitude images (f) before and (g) after the applying of positive tip voltage

According to the polarization orientations of twin domains, the domain wall directions and the relative piezoresponse intensities in PFM images can be derived, and vice versa. The PFM experimental setup in this work was schematically presented in Fig. 1(e). First, the ordinary VPFM scanning was performed on the $(001)_C$ surface of the PMN-0.34PT single crystal, with the reverse side grounded. Then, a selected smaller region was gradually poled using step-increased positive DC voltage $V_{dc}$ applied on the conductive tip, and the evolution of domains after each poling step was monitored by the followed VPFM imaging. It can be inferred that the upward polarizations will be reversed under positive tip voltage, as sketched with blue arrows in Fig. 1(e). In the following sections, the VPFM phase and amplitude images will exhibit the details of polarization switching. For example, a typical $M_C$ phase

domain pattern in a section of 10 μm × 10 μm before poling was presented in Fig. 1(f), in which, there are obvious regular $M_C$ twin domains walls along $\theta$ of 61° or 29° beside the domain walls with irregular orientations. Here, $\theta$ is the angle between the observed domain wall and the $[100]_C$ axis. When a larger area of 30 μm × 30 μm was scanned (data not shown), it was found that the ratio of domain walls with $\theta$ of 61° is much larger than that of the 29° one, indicating the predominance of the corresponding twin domains. A 5 μm × 5 μm area in Fig. 1(f) (marked with red square) which includes the former mentioned three kinds of $M_C$ domain walls was selected to be gradually poled by an external electric voltage $V_{dc}$. As an example, the domain pattern after poled by $V_{dc}$ of 5V is presented in Fig. 1(g). It could be noted that parts of the dark regions in the VPFM phase image have turned bright due to the domain switching, indicating that the out-of-plane component of the polarization vector in dark regions are pointed upward. The evolution of domain walls can also be observed on the VPFM amplitude images.

## 2. Determine of the local specific twin domains and polarization orientation of the $M_C$ phase in the initial annealed state

In order to investigate the details of the domain configuration of $M_C$ phase in the initial annealed state, the VPFM image of the selected 5 μm × 5 μm area is enlarged and presented in Fig. 2. According to the features of domain walls, this area is divided into three parts, marked as A, B and C in Fig. 2(a).

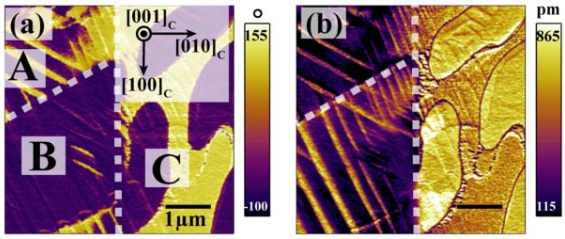


FIG. 2. (Color online) Domain pattern in the initial annealed state, (a) VPFM phase image and (b) VPFM amplitude image.

In part A, the domain walls align with $\theta$ = 61° in the initial annealed state. Both the VPFM phase (Fig. 2(a)) and amplitude (Fig. 2(b)) images consist of alternatively bright and dark

stripes, indicating that they are twin domains comprised of downward $M_C$-c ($M_C$-c$\bar{1}$, $M_C$-c$\bar{2}$, $M_C$-c$\bar{3}$ or $M_C$-c$\bar{4}$) and upward $M_C$-a ($M_C$-a1 or $M_C$-a$\bar{3}$) domain variants. On the other hand, in the original annealed state of part B, the domain wall is dominated with $\theta$ = 29°. The VPFM phase image is totally dark (Fig. 2(a)) but the PFM amplitude image is alternatively dark and bright (Fig. 2(b)), which indicates that the twin domains consist of upward $M_C$-c ($M_C$-c1, $M_C$-c2, $M_C$-c3 or $M_C$-c4) and upward $M_C$-a/b ($M_C$-a1, $M_C$-a$\bar{3}$, $M_C$-b1 or $M_C$-b$\bar{3}$). What's more, there are domain walls with irregular orientations in part C, the VPFM phase of domain variants on two sides of such domain walls show strikingly contrast, but the VPFM amplitude of them are almost the same, indicating that they are 180° domain walls between $M_C$-c domains.

The number of possible polarization orientations in the selected area is greatly reduced by the above analysis, but the twin domains have not been specifically identified. When the multi-domain state was formed in the single crystal with low-symmetry ferroelectric phase, the strain compatibility conditions must be satisfied, as a result, the domain walls will align along some defined directions [55, 56]. In the following, based on the vector relation between different polarizations and the formation rules of domain walls, the specific twin domains in part A and B of the selected area will be clarified, and the polarization orientations of the $M_C$ phase in this sample will also be determined.

As sketched in Fig. 3(a), the angle between $M_C$ and T phase polarizations is set as $\alpha$, and the deviation distance between their end in the pseudo-cubic unit cell is set as $a$, where $a$=tan$\alpha$. Assuming that the polarization vectors on the two sides of the twin domain wall are $\overrightarrow{MC_1}$ and $\overrightarrow{MC_2}$, whose coordinates are set to be ($x_1$, $y_1$, $z_1$) and ($x_2$, $y_2$, $z_2$). Before poling, we just consider uncharged domain walls due to the lower domain wall energy, as sketched with violet plane in Fig. 3(a). Based on the formation rule of domain walls, the expression of domain wall angle $\theta$ scanned on $(001)_C$ face can be derived. First, we can find out two intersection points of the domain wall plane and the $(001)_C$ face. Because $|\overrightarrow{MC_1}|$ and $|\overrightarrow{MC_2}|$ are equal, according to the strain boundary condition, the angle bisector of $\overrightarrow{MC_1}$ and $\overrightarrow{MC_2}$

(opposite to $\overrightarrow{MC_2}$) must be contained in the DW plane, which is defined as $\overrightarrow{IP_1}$, and the coordinate of the intersection point of $\overrightarrow{IP_1}$ and $(001)_C$ face can be expressed by $\overrightarrow{MC_1}$ and $\overrightarrow{MC_2}$. Besides, the domain wall planes will be perpendicular to the plane formed by these two polarizations. So, there must be a line on the domain wall plane which is perpendicular to both $\overrightarrow{MC_1}$ and $\overrightarrow{MC_2}$, and this line is defined as $\overrightarrow{IP_2}$, which can also been expressed by $\overrightarrow{MC_1}$ and $\overrightarrow{MC_2}$. The line on $(001)_C$ face determined by $\overrightarrow{IP_1}$ and $\overrightarrow{IP_2}$ is the intersection line ($\overrightarrow{IL}$) of domain wall and the $(001)_C$ plane, which can be expressed as

$$\overrightarrow{IL} = \overrightarrow{IP_2} - \overrightarrow{IP_1} = \left(\frac{z_2 \cdot y_1 - z_1 \cdot y_2}{x_1 \cdot y_2 - x_2 \cdot y_1} - \frac{x_1 - x_2}{z_1 - z_2}, \frac{z_1 \cdot x_2 - z_2 \cdot x_1}{x_1 \cdot y_2 - x_2 \cdot y_1} - \frac{y_1 - y_2}{z_1 - z_2},\ 0\right) \quad (1)$$

And the domain wall angle can be expressed as,

$$\tan\theta = \frac{y_{IL}}{x_{IL}} = \left(\frac{z_1 \cdot x_2 - z_2 \cdot x_1}{x_1 \cdot y_2 - x_2 \cdot y_1} - \frac{y_1 - y_2}{z_1 - z_2}\right) \Big/ \left(\frac{z_2 \cdot y_1 - z_1 \cdot y_2}{x_1 \cdot y_2 - x_2 \cdot y_1} - \frac{x_1 - x_2}{z_1 - z_2}\right) \quad (2).$$

The coordinate of each possible polarization as shown in Fig. 3(b) and 3(c) can be write as $M_C$-c1 (a, 0, 1), $M_C$-a1 (1, 0, a), etc. We have plugged the coordinates of possible twin domains into formula (2), so that the curves of $\theta$ versus $\alpha$ ($\theta$-$\alpha$) with $\alpha$ varies from 0° to 45° are obtained. The $\theta$-$\alpha$ curves for possible $M_C$-c/$M_C$-a (Fig. 3(b)) twin domains are presented in Fig. 3(d). As marked with red circles, some of $M_C$-c/$M_C$-a twin domains can form domain walls with $\theta$ = 61°, which have appeared in part A, corresponding to the twin domains of $M_C$-c$\bar{2}$/$M_C$-a1 or $M_C$-c$\bar{4}$/$M_C$-a$\bar{3}$. Additionally, the corresponding value of $\alpha$ is determined to be 29°. However, as can be seen in Fig. 3(d), it is impossible for the $M_C$-c and $M_C$-a1/3 (Fig. 3(b)) to form twin domain walls with $\theta$ = 29°, which is the dominating domain wall orientation in part B, indicating that it is not $M_C$-c/$M_C$-a twin domains in part B before poling. The $\theta$-$\alpha$ curves of possible $M_C$-c/$M_C$-b (Fig. 3(c)) twin domains are presented in Fig. 3(g), there are domain walls with $\theta$ = 29° formed by $M_C$-c/$M_C$-b twin domains as marked by green circles, which are $M_C$-c3/$M_C$-b1 or $M_C$-c1/$M_C$-b$\bar{3}$ twins, also corresponding to $\alpha$ of 29°.

Although we have determined two possible couples of $M_C$ twin domains in both part A and B, the interaction lines of their corresponding domain walls with $(001)_C$ plane are the same.

In the following section, we will just discuss the twin domains of $M_C$-$c\bar{2}$/$M_C$-a1 in part A and $M_C$-c3/$M_C$-b1 in part B. The schematic drawing of domain wall plane between $M_C$-$c\bar{2}$ and $M_C$-a1 domains is presented in Fig. 3(e), and the corresponding domain wall orientation observed on the $(001)_C$ surface of the sample is showed in Fig. 3(f). Similarly, the domain wall plane formed between $M_C$-c3 and $M_C$-b1 domains is sketched in Fig. 1(h), and the domain walls observed on the $(001)_C$ surface is showed in Fig. 3(i).

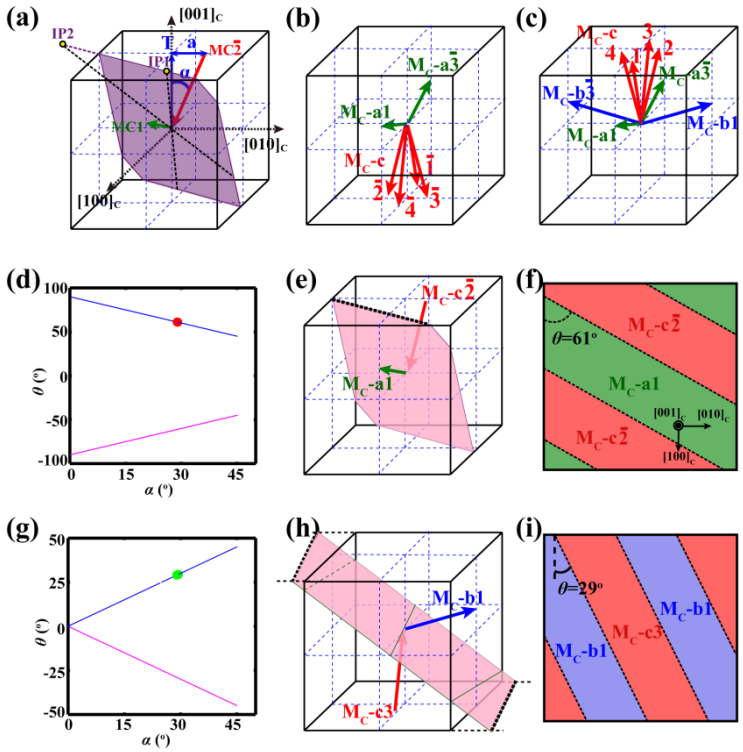


FIG. 3. (Color online) Schematic diagram of (a) uncharged domain wall, (b) possible domain variants in part A, (c) possible domain variants in part B. (d) $\theta$ -$\alpha$ curves for possible $M_C$-c/$M_C$-a twin domains, (e) schematic diagram of domain wall plane between $M_C$-$c\bar{2}$ and $M_C$-a1 domains, (f) schematic diagram of domain wall orientation between $M_C$-$c\bar{2}$ and $M_C$-a1 domains observed on the $(001)_C$ surface, (g) $\theta$ -$\alpha$ curves for possible $M_C$-c/$M_C$-b twin domains, (h) schematic diagram of domain wall plane between $M_C$-c3 and $M_C$-b1 domains, (f) schematic diagram of domain wall orientation between $M_C$-c3 and $M_C$-b1 domains observed on the $(001)_C$ surface.

In addition, around the domain walls, there will be lattice mismatch because of the lattice distortion. In order to reduce the strain energy, the crystal lattices will be inclined; as a result, the domain wall orientations will be slightly changed. The incline manner and exact angles of the crystal lattices can be obtained from the X-ray diffractive 3D-RSM results [48], and the incline angle is so small that we have neglect this factor here.

### 3. Switching process of different kinds of $M_C$ domains under step-increased $V_{dc}$

After clarification of the specific twin domains in some selected area, this area was gradually poled by step-increased $V_{dc}$ in order to investigate the switching process and features of different $M_C$ domains under various electric histories. The VPFM amplitude and phase images obtained after each poling step are presented sequentially in Fig. 4. In the following text, the domain evolution process in parts A, B and C will be discussed in detail, separately.

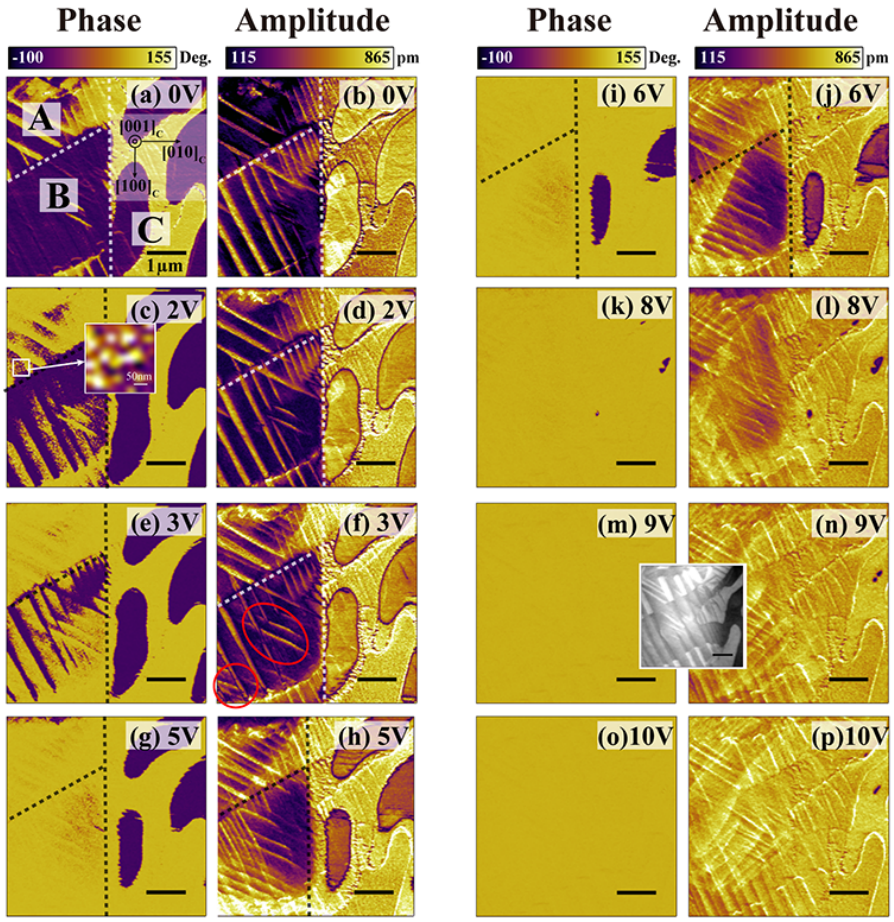


FIG. 4. (Color online) Domain evolution under step-increased tip voltage

In part A, after poled under $V_{dc}$ = 2V, some polarizations in the $M_C$-a1 domains begin to reverse, and there are nanodomains with radius of 30-50 nm emerged in the section of $M_C$-a1 domains (Fig. 4(c)), indicating that the polarization switching in $M_C$-a1 twins initiated by the nucleation of reversed polarization domains throughout the $M_C$-a1 region. Bigger volume fraction of $M_C$-a1 domains is reversed with the increasing $V_{dc}$. When $V_{dc}$ is increased to a value higher than 3V (Fig. 4(f)), the number of domain walls began to increase, indicating that parts of $M_C$-a1 domains have been switched to $M_C$-c$\bar{2}$ domains. The density of such twin domain walls achieved its maximum after poled by $V_{dc}$ = 5V (Fig. 4(h)). Meanwhile, the VPFM phase image totally became bright (Fig. 4(g)), indicating that all of the $M_C$-a1 domains in part A have been reversed. And the electrical neutral domain walls have turned to charged domain walls between $M_C$-a$\bar{1}$ and $M_C$-c$\bar{2}$ domain variants. It should be noticed that, until now, the dominant domain wall direction in part A is not changed and there are no obvious intermediate domain wall orientations, indicating that the polarization direction of original $M_C$-c domains is not changed by the tip voltage. In our poling and imaging condition, the switching from $M_C$-a1/a$\bar{1}$ to $M_C$-c$\bar{2}$ domain seems like a sudden change, no gradually rotation process is observed**.** When $V_{dc}$ is higher than 8V, the original twin domain walls with $\theta$ = 61° become blurry, and the VPFM phase image turned to nearly a monocolor (Fig. 4(m)), indicating that more volume of $M_C$-a1 domains have switched to $M_C$-c$\bar{2}$ domains. Please note that there are some profiles look like domain walls with $\theta$ = 61° in Fig. 4(n) and 4(p), which should be attributed to the influence of topography of the sample surface as shown in the inset between Fig. 4(m) and 4(n).

In part B, analogous to the $M_C$-a1 domains in part A, parts of polarizations in $M_C$-b1 domains begin to switch after poled by $V_{dc}$ = 2V and some reversed nanodomains appear (Fig. 4(c)), indicating that the switching of domains also nucleated from many points in $M_C$-b1 domains. Although the out-of-plane polarization vector component of $M_C$-c3 domains in part B also point upward, the polarizations in the $M_C$-c3 domains did not switch under the 2V tip voltage, implying that the switching of the $M_C$-c domain is more difficult than in the $M_C$-a/b domain under such tip voltage. After poled by a $V_{dc}$ of 3V, as marked by red circles in Fig.

4(f), a small volume fraction of original twin domain walls with $\theta = 61°$ is expanded, and more of such domain walls appeared in other areas of part B as well, indicating the appearance of $M_C$-c/$M_C$-a twin domains. The switching from $M_C$-c3/$M_C$-b1 to $M_C$-c/$M_C$-a twin domains in part B should be attributed to the overlap of domains in the thickness direction of the sample. As there are bigger volume fraction of $M_C$-c/$M_C$-a twin domains in the sample, when the external $V_{dc}$ is applied, more layers of domains will response, and the small volume fraction of $M_C$-c/$M_C$-b twin domains on the sample surface will be affected. Meanwhile, the width of the original $M_C$-c3 domains become narrow (Fig. 4(f)), indicating that the original upward $M_C$-c3 domains begin to switch from the twin domain walls. When $V_{dc}$ is increased to 5V, the density of domain walls in part B also achieved the maximum. When the tip voltage is further increased, the domain evolution in part B shows a similar character as that in part A.

In part C, when $V_{dc}$ is increased beyond 3V, the polarizations in the upward $M_C$-c domain variants start to reverse from the 180° domain walls (Fig. 4(e) and 4(f)), which is different from the $M_C$-a/b domains in parts A and B. As $V_{dc}$ is further increased, the volume fraction of upward $M_C$-c domains shrinks gradually while the section of downward $M_C$-c domains expands. When $V_{dc}$ is increased beyond 8V, part C is poled into a single domain state.

Additionally, as can be seen in Fig. 4(b) and 4(p), after poled by a $V_{dc}$ of 9V, some wedged domains with the center line along the direction -45° to the $[100]_C$ axis appeared in parts A and B. And it is notable that, as the wedged domain walls moved to the left side of part B, the right side of part B changed to the same as part C (Fig. 4(p)), indicating that the appearance of such wedged domain walls should be attributed to the expansion of the single domain area in part C and the formation of charged domain walls between different downward $M_C$-c domain variants in part B and C.

## IV. SUMMARY AND CONCLUSIONS

In summary, the twin domains and the tip-voltage-induced domain switching of $M_C$ phase in the PMN-0.34PT single crystal was revealed by PFM. Based on the scanned domain patterns and the formation rules of domain walls, the specific twin domains have been

clarified for some typical areas, which were $M_C$-$c\bar{2}$/$M_C$-a1 or $M_C$-$c\bar{4}$/$M_C$-$a\bar{3}$ in part A, $M_C$-c3/$M_C$-b1 or $M_C$-c1/$M_C$-$b\bar{3}$ in part B, and the polarization orientation of the $M_C$ phase in this sample was determined to be 29° from the $<001>_C$ directions. The switching process and features of $M_C$-a, $M_C$-b and $M_C$-c domains under the step-increased PFM tip voltage $V_{dc}$ were explicitly revealed. It was found that the switching of $M_C$-a/b nucleating throughout the volume of the whole domains, the switching of $M_C$-c domains start from domain walls, and the switching of $M_C$-a to $M_C$-c domains was observed to be a sudden process. The results of this work not only provide an insight into the domain structure of monoclinic $M_C$ phase in piezoelectric single crystal with MPB, a more clear understanding of domain switching process under PFM tip voltage, but also help establish an improved structure model which is important for theoretical investigation and computer simulations.

## ACKNOWLEDGMENTS

This research was supported by the National key Basic Research Program of China (No. 2013CB632900). Z. Luo acknowledges the National Natural Science Foundation of China (11374010, 11434009). The synchrotron diffraction measurements were performed on 12-ID-D beamline of Advanced Photon Source at Argonne National Laboratory, which is supported by the DOE, Basic Energy Sciences, under Contract No. DE- AC02-06CH11357.

## References


[1] S. E. Park and T. R. Shrout, J. Appl. Phys. **82**, 1804 (1997).

[2] S. Liu, S. E. Park, T. R. Shrout, and L. E. Cross, J. Appl. Phys. **85**, 2810 (1999).

[3] R. Zhang, B. Jiang, and W. Cao, J. Appl. Phys. **90**, 3471 (2001).

[4] H. Fu and R. E. Cohen, Nature **403**, 281-283 (2000).

[5] Y. Jin, Y. Wang, and A. G. Khachaturyan, Phys. Rev. Lett. **91**, 197601 (2003).

[6] G. Xu, J. Wen, C. Stock, and P. M. Gehring, Nat. Mater. **7**, 562 (2008).

[7] F. Li, S. Zhang, Z. Xu, X. Wei, J. Luo, and T. R. Shrout, J. Appl. Phys. **108**, 034106 (2010).

[8] T. Sluka, A. K. Tagantsev, D. Damjanovic, M. Gureev, and N. Setter, Nat. Commun. **3**, 748 (2012).

[9] B. Noheda, D. E. Cox, G. Shirane, J. A. Gonzalo, L. E. Cross, and S.-E, Park, Appl. Phys. Lett. **74**, 2059 (1999).

[10] D. Vanderbilt and M. H. Cohen, Phys. Rev. B **63**, 094108 (2001).

[11] E. Sun and W. Cao, Prog. Mater. SCI. **65**, 124-210 (2014).

[12] Z. Ye, B. Noheda, M. Dong, D. Cox, and G. Shirane, Phys. Rev. B **64**, 184114 (2001).

[13] J. M. Kiat, Y. Uesu, B. Dkhil, M. Matsuda, C. Malibert, and G. Calvarin, Phys. Rev. B **65**, 064106 (2002).

[14] P. Bao, F. Yan, X. Lu, J. Zhu, H. Shen, Y. Wang, and H. Luo, Appl. Phys. Lett. **88**, 092905 (2006).

[15] B. Noheda, D. E. Cox, G. Shirane, J. Gao, and Z. Ye, Phys. Rev. B **66**, 054104 (2002).

[16] A. K. Singh and D. Pandey, Phys. Rev. B **67**, 064102 (2003).

[17] R. Guo, L. E. Cross, S-E. Park, B. Noheda, D. E. Cox, and G. Shirane, Phys. Rev. Lett. **84**, 5423 (2000).

[18] E. H. Kisi, T. O. Piltz, J. S. Forrester, and C. J. Howard, J. Phys.: Condens. Matter. **15**, 3631 (2003).

[19] M. Ahart, M. Somayazulu, R. E. Cohen, P. Ganesh, P. Dera, H. –K. Mao, R. J. Hemley, Y. Ren, P. Liermann, and Z. Wu, Nature, **451**, 545 (2008).

[20] S. Zhang and F. Li, J. Appl. Phys. **111**, 031301 (2012).

[21] S. Wada, K. Yako, H. Kakemoto, T. Tsurumi, and T. Kiguchi, J. Appl. Phys. **98**, 014019 (2005).

[22] D. Lin, H. J. Lee, S. Zhang, F. Li, Z. Li, Z. Xu, and T. R. Shrout, Scripta Mater. **64**, 1149 (2011).

[23] D. Lin, S. Zhang, Z. Li, F. Li, Z. Xu, S. Wada, J. Luo, and T. R. Shrout, J. Appl. Phys. **110**, 084110 (2011).

[24] X. Ke, D. Wang, X, Ren, and Y. Wang, Phys. Rev. B **88**, 214105 (2013).

[25] Y. Sato, T. Hirayama, and Y. Ikuhara, Appl. Phys. Lett. **104**, 082905 (2014).

[26] T. T. A. Lummen, Y. Gu, J. Wang, S. Lei, F. Xue, A. Kumar, A. T. Barnes, E. Barnes, S. Denev, A. Belianinov, M, Holt, A. N. Morozovska, S. V. Kalinin, L. Chen, and V. Gopalan, Nat. Commun. **5**, 3172 (2014).

[27] D. Damjanovic, M. Budimir, M. Davis, and N. Setter, Appl. Phys. Lett. **83**, 527 (2003).

[28] M. Davis, M. Budimir, D. Damjanovic, and N. Setter, J. Appl. Phys. **101**, 054112 (2007).

[29] D. Damjanovic, IEEE Trans Ultra Ferroelectr Freq Contr, **56**, 1574 (2009).

[30] M. D. Biegalski, K. Dorr, D. H. Kim, and H. M. Christen, Appl. Phys. Lett. **96**, 151905 (2010).

[31] M. Liu, J. Hoffman, J. Wang, J. Zhang, B. N. Cheeseman, and A. Bhattacharya, Sci. Rep. **3**, 1876 (2013).

[32] T. H. E. Lahtinen, J. O. Tuomi, and S. V. Dijken, Adv. Mater. **23**, 3187 (2011).

[33] M. Trassin, J. Phys.: Condens. Matter **28**, 033001 (2016).

[34] T. Taniyama, J. Phys.: Condens. Matter **27**, 504001 (2015).

[35] F. Bai, J. Li, and D. Viehland, Appl. Phys. Lett. **85**, 19 (2004).

[36] Y. Sato, T. Hirayama, and Y. Ikuhara, Phys. Rev. Lett. **107**, 187601 (2011).

[37] P. Gao, J. Britson, C. T. Nelson, J. T. Jokisaari, C. Duan, M. Trassin, S. H. Baek, H. Guo, L. Li, Y. Wang, Y. Chu, A. M. Minor, C. B. Eom, R. Ramesh, L. Chen, and X. Q. Pan, Nat. Commun. **5**, 3801 (2014).

[38] H. Deng, H. Zhang, X. Zhao, C. Chen, X. Wang, X. Li, D. Lin, B. Ren, J. Jiao, and H. Luo, CrystEngComm. **17**, 2872 (2015).

[39] Y. Wang, Z. Wang, W. Ge, C. Luo, J. Li, D. Viehland, J. Chen, and H. Luo, Phys. Rev. B **90**, 134107 (2014).

[40] L. Zheng, X. Lu, H. Shang, Z. Xi, R. Wang, J. Wang, P. Zheng, and W. Cao, Phys. Rev. B **91**, 184105 (2015).

[41] Y. Gu, F. Xue, S. Lei, T. T. A. Lummen, J. Wang, V. Gopalan, and L. Chen, Phys. Rev. B **90**, 024104 (2014).

[42] F. Fang, X. Luo, and W. Yang, J. Am. Ceram. Soc. **96**, 228 (2013).

[43] N. Zhang, H. Yokota, A. M. Glazer, Z. Ren, D. A. Keen, D. S. Keeble, P. A. Thomas, and Z. Ye, Nat. Commun. **5**, 5231 (2014).

[44] L. Zheng, Y. Jing, X. Lu, R. Wang, G. Liu, W. Lu, R. Zhang, and W. Cao, Phys. Rev. B **93**, 094104 (2016).

[45] Y. Jin, Y. Wang, A. G. Khachaturyan, J. Li, and D. Viehland, J. Appl. Phys. **94**, 5 (2003).

[46] S. Bhattacharyya, J. R. Jinschek, H. Cao, Y. Wang, J. Li, and D. Viehland, Appl. Phys. Lett. **92**, 142904 (2008).

[47] Y. Zhang, D. Xue, H. Wu, X. Ding, T. Lookman, and X. Ren, Acta Mater. **71**, 176 (2014).

[48] R. Wang, H. Xu, B. Yang, Z. Luo, E. Sun, J. Zhao, L. Zheng, Y. Dong, H. Zhou, Y. Ren, and W. Cao, Appl. Phys. Lett. **108**, 152905 (2016).

[49] M. Trassin, G. D. Luca, S. Manz, and M. Fiebig, Adv. Mater. **27**, 4871 (2015).

[50] S. A. Denev, T. T. A. Lummen, E. Barnes, A. Kumar, and V. Gopalan, J. Am. Ceram. Soc. **94**, 2699 (2011).

[51] V. V. Shvartsman, B. Dkhil, and A. L. Kholkin, Annu. Rev. Mater. Res. **43**, 423 (2013)

[52] Z. Yin, H. Luo, P. Wang, and G. Xu, Ferroelectrics **229**, 207 (1999).

[53] Z. Luo, Z. Chen, T. Yang, H. Liu, C. Huang, H. Huang, H. Wang, M. Yang, C. Hu, G. Pan, W. Wen, X. Li, Q. He, T. Sritharan, Y. Chu, L. Chen, and C. Gao, Phys. Rev. B **88**, 064103 (2013).

[54] Z. Luo, H. Huang, H. Zhou, Z. Chen, Y. Yang, L. Wu, C. Zhu, H. Wang, M. Yang, S. Hu, H. Wen, X. Zhang, L. Chen, D. Fong, and C. Gao, Appl. Phys. Lett. **104**, 182901 (2014).

[55] W. Cao, and L. E. Cross, Phys. Rev. B **44**, 5 (1991).

[56] J. Sapriel, Phys. Rev. B **12**, 11 (1975).

## Figure captions:

**FIG. 1.** (Color online) (a) Spontaneous polarization orientations of $M_C$ phase, (b) simulation result of (00L) diffraction pattern on H0L plane, (c) X-ray diffractive 2D-RSM around (004) Bragg spot on H0L reciprocal plane, the diffraction intensity was indicated by different color (low to high: blue, green, yellow, red), (d) synchrotron X-ray diffractive 3D-RSM around (006) diffraction spot (Reuse of [Applied Physics Letters 108, 152905 (2016), Fig. 2f], with the permission of AIP Publishing), the diffraction intensity was indicated by different color (low to high: yellow, pink, purple). (e) Schematic diagram of PFM setup, VPFM phase and amplitude images (f) before and (g) after the applying of positive tip voltage

**FIG. 2.** (Color on line) Domain pattern in the initial annealed state, (a) VPFM phase image and (b) VPFM amplitude image.

**FIG. 3.** (Color online) Schematic diagram of (a) uncharged domain wall, (b) possible domain variants in part A, (c) possible domain variants in part B. (d) $\theta$ -$\alpha$ curves for possible $M_C$-c/$M_C$-a twin domains, (e) schematic diagram of domain wall plane between $M_C$-$c\bar{2}$ and $M_C$-a1 domains, (f) schematic diagram of domain wall orientation between $M_C$-$c\bar{2}$ and $M_C$-a1 domains observed on the $(001)_C$ surface, (g) $\theta$ -$\alpha$ curves for possible $M_C$-c/$M_C$-b twin domains, (h) schematic diagram of domain wall plane between $M_C$-c3 and $M_C$-b1 domains, (f) schematic diagram of domain wall orientation between $M_C$-c3 and $M_C$-b1 domains observed on the $(001)_C$ surface.

**FIG. 4.** (Color on line) Domain evolution under step-increased tip voltage